Seismic Safety Analysis of Concrete Arch Dams Based on Combined Discrete Crack and Plastic–Damage Technique

O. Omidi & V. Lotfi
Amirkabir University of Technology, Iran

SUMMARY:
There are different techniques to examine the non-linear seismic behavior of concrete arch dams, among which, discrete crack (DC) method is the most popular mainly for simulation of its pre-existing joints. A more recent option introduced for mass concrete modeling is plastic–damage (PD) approach. In this study, a special finite element program called SNACS is developed based on the combined discrete crack and plastic–damage technique. Basic concepts of the methods are explained initially. Subsequently, including dam–reservoir interaction, the nonlinear dynamic analysis of a typical arch dam is examined by the combined technique and the results are compared against the single methods. Overall, DC–PD model is found to be a more rigorous, consistent and realistic approach from different aspects in comparison with both DC and PD models alone. Therefore, the DC–PD technique could be considered as a major step toward more accurate seismic safety evaluation of concrete arch dams.

Keywords: plastic–damage; discrete crack; arch dam; dam–water interaction; seismic safety

1. INTRODUCTION

There have been increasing attentions to the seismic safety of concrete dams as one of the main infrastructures needed for flood control or water supply in recent years, because it is increasingly evident that the seismic design concepts utilized at the time of construction of most existing dams were simplistic and inadequate. Furthermore, the population at risk located downstream of dams continues to expand. Therefore, collapse of dams would cause a socio-economic tragedy. The growing concern of the seismic safety of such vital structures has caused great interest for re-evaluating existing dams using nonlinear models to predict crack initiation and its propagation through dam body.

The dynamic analysis of arch dams should consider the following factors (Chopra 2008): dam–water interaction, wave absorption at the reservoir boundary, water compressibility, dam–foundation interaction, spatially-varying ground motion around the canyon, vertical contraction and peripheral joints opening and slippage and finally a possible cracking in mass concrete monoliths. Concrete modeling of arch dams are commonly categorized into two different approaches as discrete and continuum models. Contraction joint opening in arch dams during an earthquake has been studied for years (Fenves *et al.* 1992; Ahmadi and Razavi 1992; Lau *et al.* 1998; Ahmadi *et al.* 2001; Azmi and Paultre 2002; Arabshahi and Lotfi 2009). Moreover, several studies have addressed the nonlinearity of concrete material of arch dams (Lee and Fenves 1998b; Valliappan *et al.* 1999; Gunn 2001a,b; Espandar *et al.* 2003; Mirzabozorg and Ghaemian 2005). Although the behavior of arch dams while either the joints are simulated or the body is monolithically analyzed by employing a constitutive concrete model seems well understood, knowledge of their combination while both joints and concrete blocks nonlinearities considered in a single analysis is rather limited and needs more consideration.

Although mass concrete structures, such as arch dams, are governed by multiaxial stress states, their safety is commonly evaluated based on a uniaxil extent (Valliappan et al. 1999; Gunn 2001a,b;

Espandar *et al.* 2003; Mirzabozorg and Ghaemian 2005). Most of smeared crack and damage mechanics models are established on the principal stress failure envelope. To assess the safety of such a mass concrete problem more realistically, a multiaxial failure envelope with a relevant stress path to failure needs to be addressed. The plastic–damage concrete model three dimensionally implemented herein had been successfully employed for seismic fracture analysis of concrete gravity dams in a 2-D plane stress implementation by Lee and Fenves in 1998. The model is able to simulate compressive crushing as well as tensile cracking and post-cracking behavior. Furthermore, it provides for the stiffness degradation induced by plastic straining, both in tension and compression. Despite these recent advances in academic research, less attention is focused on the application of plastic–damage models in analysis of concrete arch dams, especially under seismic loadings.

2. DISCRETE CRACK MODEL

Discrete crack model implemented herein employs zero thickness interface elements having suitable constitutive laws for the two different applications in contraction and perimeter joints. The joints' constitutive relationships used in this study have been successfully utilized previously (Lotfi and Espandar 2004). However, the basic concepts in each option are briefly presented below.

2.1. Separation with linear shear mechanism

This is the option in which joints can open and close during the analysis but are not allowed to slide. It is suitable for the contraction joints with unbeveled shear keys of considerable height. This kind of joints is embedded in the body of arch dams located in seismically active region. Fig. 2.1 illustrates the local stress-strain relationship for this option before and after the first opening.

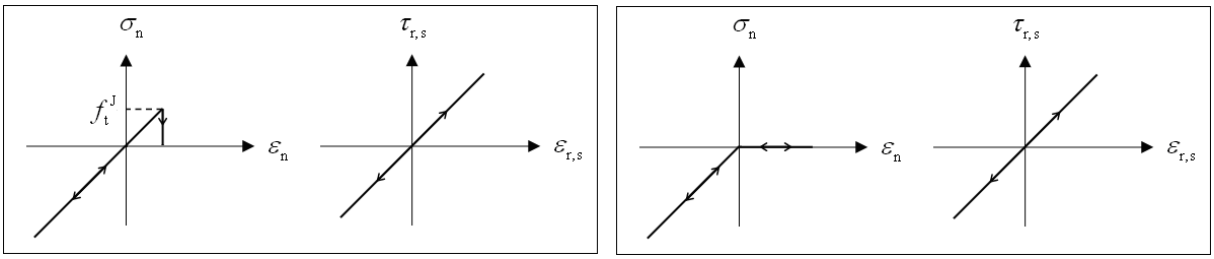

Figure 2.1. Local stress-strain relationship for the case of opening without sliding: before the first opening (left) and after the first opening (right)

2.2. Separation with shear release mechanism

A simplified practical model of sliding previously examined in application of concrete arch dams is utilized to account for shear slippage at perimeter joints. This is also a more realistic model for contraction joints without shear keys. Perfect tensile and shear softening is assumed in this option. This can also be seen as an approximate slippage model. In fact, the friction angle is assumed 90 degrees. Meanwhile, as depicted in Fig. 2.2, it also retrieves its shear stiffness coefficients similar to the normal direction.

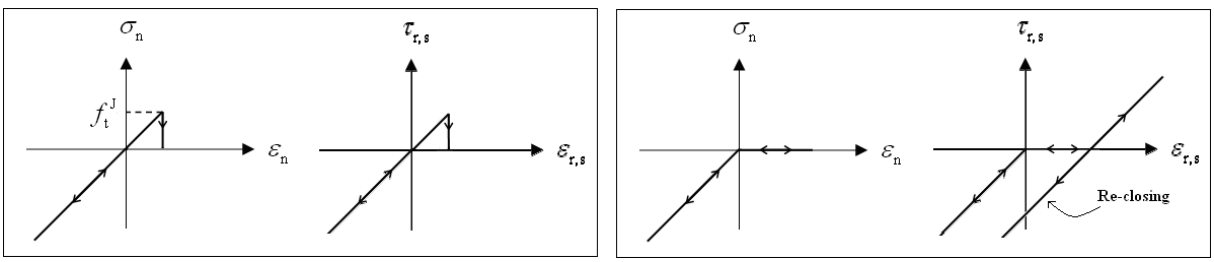

Figure 2.2. Local stress-strain relationship for the case of opening with simple sliding: before the first opening (left) and after the first opening (right)

3. PLASTIC–DAMAGE MODEL

The plastic–damage model proposed by Lee and Fenves (1998a) and successfully employed in 2-D applications on gravity dams is implemented for three-dimensional stress space (Omidi 2010). This model includes tensile and compressive damage variables to account for the two distinct phenomena of cracking and crushing which usually occur in concrete under cyclic loadings.

3.1. Constitutive relationships

3.1.1. Backbone plastic–damage model
The basic ingredients of the inviscid plastic–damage model as the backbone model are:

$$\begin{aligned} &\boldsymbol{\varepsilon} = \boldsymbol{\varepsilon}^{\mathrm{e}} + \boldsymbol{\varepsilon}^{\mathrm{p}} \;; \quad \boldsymbol{\sigma} = (1-D)\,\bar{\boldsymbol{\sigma}} \;; \quad \bar{\boldsymbol{\sigma}} = \mathbf{E}_0 : \boldsymbol{\varepsilon}^{\mathrm{e}} \\ &\dot{\boldsymbol{\varepsilon}}^{\mathrm{p}} = \dot{\lambda}\, \nabla_{\bar{\boldsymbol{\sigma}}} \Phi \;; \quad \dot{\boldsymbol{\kappa}} = \dot{\lambda}\, \mathbf{H}(\bar{\boldsymbol{\sigma}}, \boldsymbol{\kappa}) \;; \quad D = D(\bar{\boldsymbol{\sigma}}, \boldsymbol{\kappa}) \end{aligned} \tag{3.1}$$

where $\boldsymbol{\varepsilon}$, $\boldsymbol{\varepsilon}^{\mathrm{e}}$ and $\boldsymbol{\varepsilon}^{\mathrm{p}}$ are the total, elastic and plastic strains, respectively; $\boldsymbol{\sigma}$ and $\bar{\boldsymbol{\sigma}}$ are the stress and the effective stress tensors, respectively; $\mathbf{E}_0$ is the initial (undamaged) elastic stiffness tensor; Φ is the flow potential function; D is the stiffness degradation variable and $\mathbf{H}$ is the plastic modulus vector derived considering plastic dissipation. Moreover, $\boldsymbol{\kappa}$ is the plastic–damage vector containing the normalized plastic–damage variables in tension and compression (i.e., $\boldsymbol{\kappa} = \{\kappa_{\mathrm{t}}, \kappa_{\mathrm{c}}\}^{\mathrm{T}}$) which play the role of the hardening variables (Lee and Fenves 1998a; Omidi and Lotfi 2010, 2012).

3.1.2. Yield condition and flow rule
The model utilizes a yield condition based on the yield function proposed by Lubliner *et al.* (1989) and includes the modifications proposed by Lee and Fenves (1998a) to consider different evolution of strength under tension and compression. In terms of effective stresses, the yield function is:

$$F(\bar{\boldsymbol{\sigma}}, \boldsymbol{\kappa}) = f(\bar{\boldsymbol{\sigma}}, \boldsymbol{\kappa}) - c_{\mathrm{c}}(\boldsymbol{\kappa}) \;; \;\; f(\bar{\boldsymbol{\sigma}}, \boldsymbol{\kappa}) = \frac{1}{1-\alpha}\left[\sqrt{3\bar{J}_2} + \alpha\, \bar{I}_1 + \beta(\boldsymbol{\kappa})\, \langle \hat{\bar{\sigma}}_{\max} \rangle - \gamma\, \langle -\hat{\bar{\sigma}}_{\max} \rangle\right] \tag{3.2}$$

where $\hat{\bar{\sigma}}_{\max}$ is the maximum principal stress and the Macauley bracket $\langle \square \rangle$ is defined by $\langle x \rangle = (x + |x|)/2$. Besides, the parameters α, β and γ have the following definitions:

$$\alpha = \frac{(f_{\mathrm{b0}}/f_{\mathrm{c0}}) - 1}{2\,(f_{\mathrm{b0}}/f_{\mathrm{c0}}) - 1} \;; \quad \beta(\boldsymbol{\kappa}) = \frac{c_{\mathrm{c}}(\kappa_{\mathrm{c}})}{c_{\mathrm{t}}(\kappa_{\mathrm{t}})}(1-\alpha) - (1+\alpha) \;; \quad \gamma = \frac{3(1-r_{\mathrm{oct}})}{2\,r_{\mathrm{oct}} - 1} \tag{3.3}$$

where $f_{\mathrm{b0}}/f_{\mathrm{c0}}$ is the ratio of the initial yield strengths under biaxial and uniaxial compression; c_{t} and c_{c} denote the effective tensile and compressive cohesion (positive values utilized here), respectively; r_{oct} is the ratio of the octahedral shear effective stress (i.e., $\bar{\tau}_{\mathrm{oct}} = \sqrt{2\bar{J}_2/3}$) on the tensile meridian to that on the compressive meridian (i.e., $r_{\mathrm{oct}} = (\bar{\tau}_{\mathrm{oct}})_{\mathrm{TM}}/(\bar{\tau}_{\mathrm{oct}})_{\mathrm{CM}}$) at initial yield for any given $\bar{I}_1$ such that $0.5 \le r_{\mathrm{oct}} \le 1.0$. The value of $r_{\mathrm{oct}} = 2/3$ suggested by Lubliner *et al.* leads to $\gamma = 3$. Containing the parameter γ, which appears only in triaxial compression, the yield function better predicts the concrete behavior in compression under confinement. Loading/unloading conditions derived from the Kuhn–Tucker relations are given in terms of the yield function $F(\bar{\boldsymbol{\sigma}}, \boldsymbol{\kappa})$ and the plastic consistency parameter as: $\dot{\lambda} \ge 0$; $F(\bar{\boldsymbol{\sigma}}, \boldsymbol{\kappa}) \le 0$; $\dot{\lambda} F(\bar{\boldsymbol{\sigma}}, \boldsymbol{\kappa}) = 0$. The yield function is illustrated in Fig. 3.1 for plane stress state. Furthermore, a Drucker–Prager hyperbolic function is employed here as the plastic potential function:

$$\Phi = \sqrt{\beta_{\mathrm{H}}^2 + 2\bar{J}_2} + \alpha_{\mathrm{p}} \bar{I}_1 \;; \quad \beta_{\mathrm{H}} = \varepsilon_0\, \alpha_{\mathrm{p}}\, f_{\mathrm{t0}} \tag{3.4}$$

where α_p is the dilatancy parameter; f_{t0} is the maximum uniaxial tensile strength of concrete and ε_0 is the eccentricity parameter (Fig. 3.1). It is noted that the original 3-D formulation of Lee and Fenves utilizes the linear function which causes severe numerical difficulties in return-mapping process due to its apex's singularity. Such a modification, which is inevitable for the 3-D implementation, requires a part of the model to be reformulated and makes an extra iteration necessary to compute the plastic consistency parameter as the main step of the stress return algorithm (Omidi and Lotfi 2010). The model uses nonassociated flow rule, therefore requiring the solution of non-symmetric equations.

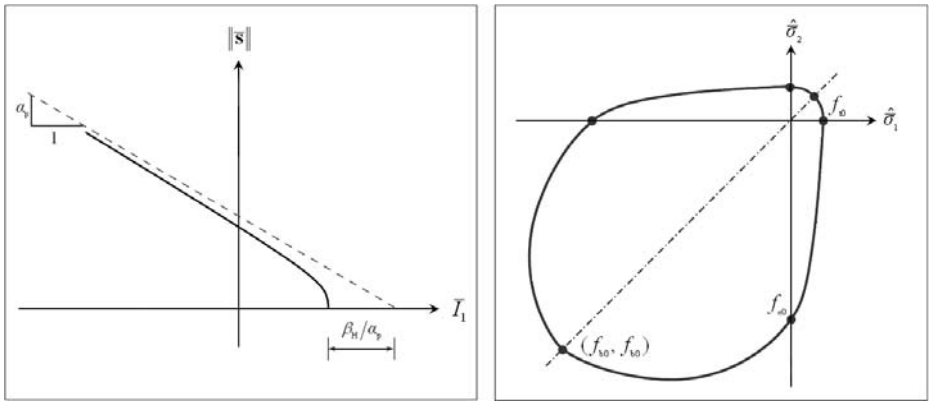

Figure 3.1. Nonassociated plasticity: flow potential in meridian plane (left) and yield surface in plane stress (right)

3.1.3. Damage and stiffness degradation

The degradation of stiffness caused by micro-cracking occurs in both tension and compression and becomes more significant as the strain increases. Under cyclic loading, the mechanism of the stiffness degradation becomes more complicated due to opening and closing of micro-cracks. The damage variables in tension and compression denoted by D_t and D_c, respectively are explicit functions of the plastic–damage variables in tension and compression introduced above. Since the model is accurately capable of capturing the two major damage phenomena, the uniaxial tensile and compressive ones, multi-dimensional degradation behavior is suggested to be evaluated by interpolating between these two main damage variables such as (Lee and Fenves 1998a):

$$D(\hat{\bar{\boldsymbol{\sigma}}}, \boldsymbol{\kappa}) = 1 - (1 - D_c(\kappa_c))(1 - s\,(\hat{\bar{\boldsymbol{\sigma}}})\, D_t(\kappa_t)) \tag{3.5}$$

where s is the stiffness recovery parameter such that $0 \le s \le 1$ and used to include the elastic stiffness recovery during elastic unloading process from tensile state to compressive state:

$$s\,(\hat{\bar{\boldsymbol{\sigma}}}) = s_0 + (1 - s_0)\, r(\hat{\bar{\boldsymbol{\sigma}}})\;; \qquad r(\hat{\bar{\boldsymbol{\sigma}}}) = \left(\sum_{i=1}^{3} \langle \hat{\bar{\sigma}}_i \rangle \right) \Big/ \left(\sum_{i=1}^{3} \left| \hat{\bar{\sigma}}_i \right| \right) \;; \qquad 0 \le r(\hat{\bar{\boldsymbol{\sigma}}}) \le 1 \tag{3.6}$$

in which, s_0 is a minimum value for s usually set to zero; the scalar quantity r is a weight factor. Following Lee and Fenves (1998b), the viscoelastic damping stress is included herein based on damage-dependent damping mechanism as $\boldsymbol{\chi}(\boldsymbol{\varepsilon}, \dot{\boldsymbol{\varepsilon}}) = \beta_R (1 - D)\mathbf{E}_0 : \dot{\boldsymbol{\varepsilon}}$ in which, β_R is a coefficient calibrated to provide a damping ratio at one natural vibration period assuming undamaged material.

3.2. Continuum large cracking

After a large amount of micro-cracking, the crack opening/closing mechanism becomes similar to discrete cracking (Lee and Fenves 1998b). The evolution equation needs to be modified to simulate large crack opening and the closing/reopening process in the continuum context as the following:

$$\tilde{\boldsymbol{\sigma}} = \mathbf{E}_0 : (\boldsymbol{\varepsilon} - \tilde{\boldsymbol{\varepsilon}}^{\mathrm{p}}) \in \left\{ \tilde{\boldsymbol{\sigma}} \mid F(\tilde{\boldsymbol{\sigma}}, \boldsymbol{\kappa}) \le 0 \right\} \;;\; \dot{\boldsymbol{\varepsilon}}^{\mathrm{p}} = (1-r)\,\dot{\tilde{\boldsymbol{\varepsilon}}}^{\mathrm{p}} \;;\; \dot{\tilde{\boldsymbol{\varepsilon}}}^{\mathrm{p}} = \dot{\lambda} \nabla_{\tilde{\boldsymbol{\sigma}}} \boldsymbol{\Phi} \;;\; r = r(\hat{\tilde{\boldsymbol{\sigma}}}) \tag{3.7}$$

where $\tilde{\boldsymbol{\varepsilon}}^{\mathrm{p}}$ is referred to as the intermediate plastic strain; r is a weight function causing the large crack modification to be applied for the states having positive principal stresses. To make the effective stress based on the plastic strain admissible in the stress space, it is necessary to employ a new damage variable denoted by D_{cr} at the crack damage corrector making the evaluated effective stress return back onto the yield surface. It is determined by the plastic consistency condition for a continued loading ($\dot{D}_{\mathrm{cr}} > 0$) such that $F((1-D_{\mathrm{cr}})\,\bar{\boldsymbol{\sigma}}, \boldsymbol{\kappa}) = 0$ from which is $D_{\mathrm{cr}} = 1 - c_{\mathrm{c}}(\boldsymbol{\kappa}) / f(\bar{\boldsymbol{\sigma}}, \boldsymbol{\kappa})$. The stiffness degradation variable is redefined considering large cracking as:

$$D = 1 - (1 - D_{\mathrm{c}})(1 - s\,D_{\mathrm{t}})(1 - s\,D_{\mathrm{cr}}) \tag{3.8}$$

The modified stress integration procedure for the large cracking states in a 3-D implementation has been detailed in (Omidi and Lotfi 2012).

3.3. Viscoplastic regularization

Some of the convergence difficulties in material models addressing softening and degradation in behavior is treated by using a viscoplastic regularization of constitutive equations. Besides, it will improve the mesh objectivity in structural simulations (Lee and Fenves 1998b). Both plastic strain and degradation variable are regularized herein by adding viscosity with the Duvaut–Lions regularization. The stress-strain relation for the viscoplastic model is given as:

$$\boldsymbol{\sigma} = (1 - D^{\mathrm{v}})\,\mathbf{E}_0 : (\boldsymbol{\varepsilon} - \boldsymbol{\varepsilon}^{\mathrm{vp}}) \;; \qquad \dot{\boldsymbol{\varepsilon}}^{\mathrm{vp}} = \frac{1}{\mu}(\boldsymbol{\varepsilon}^{\mathrm{p}} - \boldsymbol{\varepsilon}^{\mathrm{vp}}) \;;\; \dot{D}^{\mathrm{v}} = \frac{1}{\mu}(D - D^{\mathrm{v}}) \tag{3.9}$$

where $\boldsymbol{\varepsilon}^{\mathrm{vp}}$ and D^{v} are the visco-plastic strain tensor and the viscous degradation variable, respectively; μ, which is called the viscosity parameter, shows the relaxation time of the visco-plastic model and $\boldsymbol{\varepsilon}^{\mathrm{p}}$ and D are the plastic strain and degradation variable computed in the inviscid backbone model.

4. APPLICATION TO CONCRETE ARCH DAMS

The specified models are applied to Shahid Rajaee arch dam with the height of 130 m as a thin double curvature arch dam constructed on Tajan River in Sari, Iran.

4.1. Finite element simulations, material properties and loading

Details of the finite element models for both monolithic and jointed simulations are shown in Fig. 4.1. The model consists of 76 and 140, 20-node solid elements for the dam and reservoir, respectively. Moreover, 60 and 24 interface elements were also used to model the contraction and perimeter joints. The foundation is taken as rigid. This idealization was decided to reduce computational efforts. Of course, it is evident that the assumption of rigid foundation would cause large tensile stresses near the boundaries for the linear analysis. However, these high tensile stresses are expected to release, and this can be considered as a challenging test for the nonlinear model. The dynamic equilibrium equations of the dam body are quite well-known. As it is common, the mass-proportional term for the damping matrix has been omitted, because it would provide some artificial numerical stability during time marching process. The HHT method as an implicit scheme which allows for energy dissipation and second-order accuracy is employed here to integrate the governing coupled equations. The stresses needed for the restoring force vector at each step is computed based on the shifted backward-Euler scheme to keep robust numerical performance (Lee and Fenves 1998b, 2001). A pseudo-symmetric technique is utilized to solve the governing coupled dam–reservoir interaction equations (Omidi and Lotfi 2007).

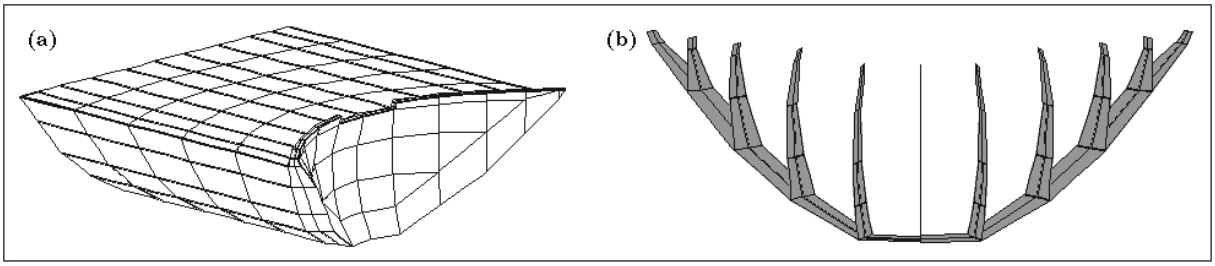

Figure 4.1. Finite element model of Shahid Rajaee arch dam: (a) 3-D view and (b) U/S view of joints

The material properties for the plastic–damage model are as: $E_0 = 30.0\,\text{GPa}$, $\nu = 0.18$, $f_t' = 3.0\,\text{MPa}$, $f_c' = -25.0\,\text{MPa}$, $G_t = 300\,\text{N/m}$, $G_c = 45000\,\text{N/m}$, $\mu = 0.15\,\Delta t$ and unit weight of 24.0 kN/m^3. Moreover, the analysis parameters are selected as $\Delta t = 0.005$ sec, $\alpha = -0.2$. In all cases carried out, the stiffness proportional damping coefficient, β_R, is determined such that equivalent damping for the fundamental frequency of vibration would be 8% of the critical damping. The reservoir bottom is partially reflective with the wave reflection coefficient equal to 0.9. Neglecting the cross-canyon excitation to have a symmetric condition, the earthquake excitations include two components of the Friuli–Tolmezzo earthquake whose records are normalized based on the frequency content for Maximum Design Earthquake (MDE) condition with the peak ground acceleration of 0.56g.

4.2. Analysis results

Four analysis cases are considered: a linear monolithic (LN) analysis, a case incorporating discrete crack (DC) model, an analysis with plastic–damage (PD) model, and the last one is the combined DC–PD case. Envelopes of maximum tensile and compressive principal stresses are obtained and the results of maximum stresses occurring on both faces are summarized in Table 4.1.

Table 4.1. Maximum principal stresses (MPa) for different cases

Case	Max. tensile principal stress (σ_1)				Max. compressive principal stress (σ_3)			
	Spillway and Middle portion		Base and Abutments		Spillway and Middle portion		Base and Abutments	
	U/S	D/S	U/S	D/S	U/S	D/S	U/S	D/S
LN	8.56	6.10	18.61	1.75	–12.40	–10.22	–4.93	–11.42
DC	2.67	7.07	3.06	3.98	–17.32	–14.25	–7.27	–15.62
PD	3.03	3.03	3.03	2.64	–13.98	–10.62	–7.62	–14.47
DC–PD	3.01	3.01	3.01	2.12	–15.04	–12.83	–7.82	–14.30

4.2.1. Linear response (LN)

For the linear analysis, it is observed that maximum tensile stresses for the spillway and abutments regions reach to maximum values of 8.56 and 18.61 MPa, respectively (Fig. 4.2). The maximum tensile principal stresses of these zones occur in the arch direction and perpendicular to the abutments as expected. Moreover, as presented in Table 4.1 and shown in Fig. 4.2, the maximum compressive stresses of this case are –12.40 and –11.42 MPa for the spillway and abutments regions, respectively.

4.2.2. Discrete crack analysis (DC)

For case DC, the maximum tensile stress for the whole analysis is limited to 7.07 MPa, which occurs approximately 25 m below the spillway on the downstream face (Fig. 4.2). It is clear that high tensile stresses in the spillway and abutments regions observed in the linear analysis are released in this case by opening of the joints near to these regions. However, as the central cantilevers move toward upstream, a maximum tensile stress of 7.07 MPa develops in the cantilever direction on downstream face. Of course, this limited stress is still higher than the tensile strength of working joints or mass concrete itself.

4.2.3. Plastic–damage analysis (PD)

The envelopes of maximum tensile and compressive stresses throughout the plastic–damage analysis are depicted in Fig. 4.2. In the linear analysis, it was noticed that very high tensile stresses were computed at the base of the dam due to the rigid foundation assumption. In addition, high tensile stresses occurred in the spillway region in arch direction, which in reality are released with the opening of contraction joints. It is observed that the plastic–damage model has completely bounded the amount of tensile stresses to a value close to the tensile strength of concrete. In this regard, slight overstressing of tensile stresses (about 1%) is still noticed in the dam body for this case, due to three-dimensional stress states effects.

Furthermore, the tensile and compressive damages obtained for different regions of the dam body at the end of analysis are illustrated in Fig. 4.3. The regions undergoing shear damage experience both tensile and compressive damage simultaneously. Shear damage occurring in these zones are due to multiaxial stress states.

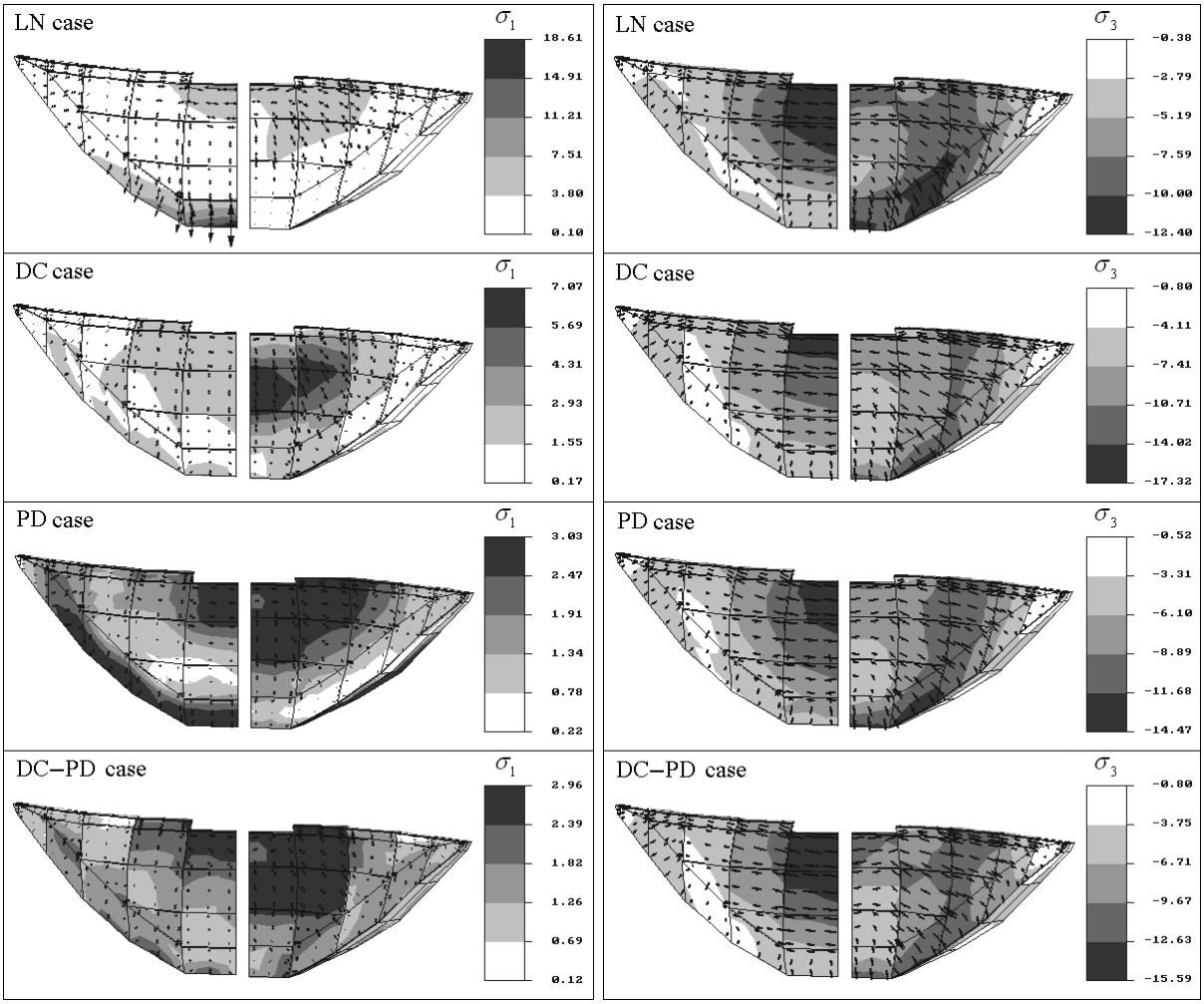

Figure 4.2. Envelopes of principal stresses (MPa) for all cases: tension (left) and compression (right)

4.2.4. Combined discrete crack and plastic–damage technique (DC–PD)

This subsection presents the seismic response of Shahid Rajaee arch dam with combined discrete crack and plastic–damage technique. The objective of the analysis is to investigate the nonlinear effects due to the presence of contraction and perimeter joints at predefined regions of the dam combined with possible cracking of concrete cantilever blocks. Fig. 4.2 illustrates the envelopes of maximum tensile stresses and maximum compressive stresses for the combined case. It is observed that the distribution on the upstream face is different with PD model and similar to DC model.

However, for downstream face, it is closer to the PD results. This means that opening of contraction and perimeter joints are influencing this distribution significantly on the upstream face. The maximum tensile stress on the whole dam body is 2.96 MPa occurring in the spillway on upstream face and the middle portion of the dam body on downstream face. Meanwhile, the magnitude of maximum tensile stress on the upstream face of the base and abutment regions is much lower than for case PD, and it is close to the case DC. This reveals that opening of perimeter joint is the dominant behavior for limiting tensile stresses in this region.

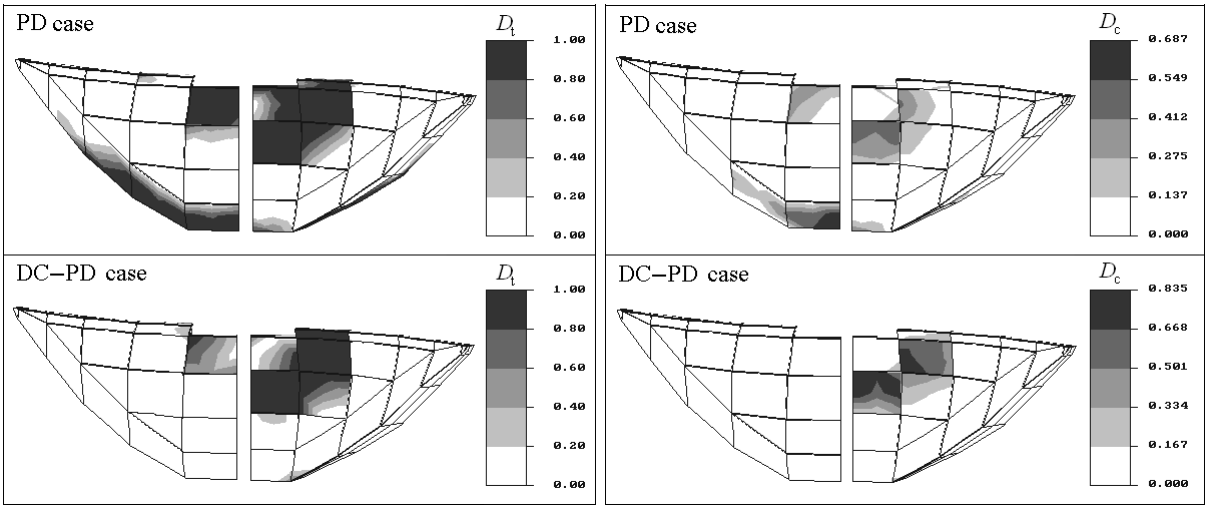

Figure 4.3. Damage distribution in PD and DC–PD cases: tensile damage (left) and compressive damage (right)

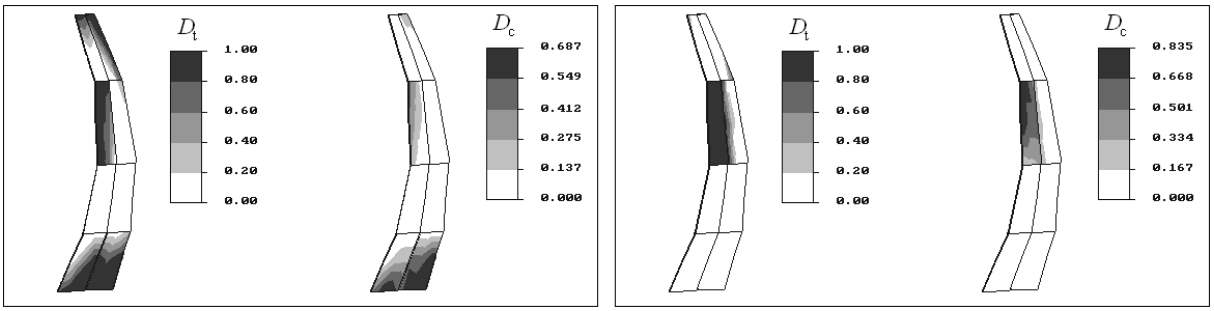

Figure 4.4. Damage variables through thickness of the crown cantilever: PD case (left) and DC–PD case (right)

Furthermore, the tensile and compressive damages for case DC–PD are depicted in Fig. 4.2 and Fig. 4.3. The extent of damage occurring in the thickness of the crown cantilever indicates that the tensile damage has extended to about half of the thickness in several locations. The plots of damage patterns exhibit similar extent on the downstream face, which is concentrated in the middle portion and adjacent to the spillway region. However, for the upstream face, case DC–PD shows less damage in the spillway region. Meanwhile, there is no damage in the upstream face of the base and abutment regions for case DC–PD, even though significant damage cracking occurred in this region for case PD.

Comparison of the stream and vertical crest displacements between the results of the PD and DC–PD cases and those of the linear or DC cases (Fig. 4.5) shows a drift in the crest displacements in upward and upstream directions. This is the main characteristic of displacement histories in plastic–damage approach, which is due to extensive cracking of downstream face of the dam beneath the crest.

Not exposing large displacements in the dam under the severe earthquake excitations considered, the analyses give an initial sign of a safe design of the dam based on the adopted theories and assumptions.

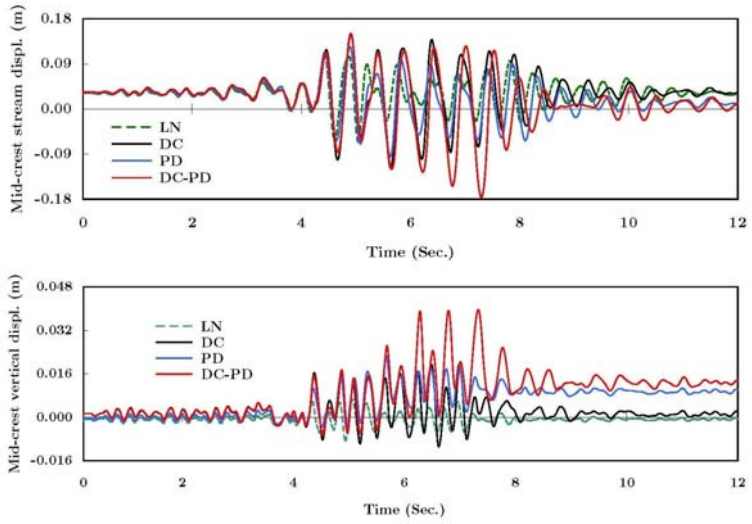

Figure 4.5. Stream and vertical displacements at the mid-crest point for all cases

5. CONCLUSIONS

A special finite element program called SNACS was developed to study the damage-induced dynamic response of concrete arch dams including water compressibility effects. The program employs a plastic–damage model modified for large crack opening/closing possibility and a discrete crack model based on two shear mechanisms. An idealized symmetric model of the 130 m high Shahid Rajaee arch dam in Iran is considered due to the Friuli–Tolmezzo earthquake components. Four cases are analyzed; a linear case (LN) and three nonlinear cases based on the plastic–damage model (PD), the discrete crack model (DC) and finally combined case (DC–PD). The main conclusions are summarized as follows.

The results of the PD and DC–PD cases show that the arch dam can suffer significant damage during a strong earthquake and still remains stable. The maximum tensile stresses on the upstream face of the base and abutments regions for the DC–PD model are much lower than a similar value for the PD approach and it is close to the DC model. This reveals that opening of perimeter joints is the dominant behavior for limiting tensile stresses in this region. The distribution and maximum values of dominant compressive stresses in different regions for the DC–PD model depart from PD results and become more similar to DC model.

The major drift toward upstream and vertical directions which is usually noticed as the prominent characteristic of displacements history in PD approach is slightly increased in the DC–PD case due to more extensive damage at downstream face below the spillway. Comparing PD and DC–PD cases from damage pattern point of view, it is observed that the DC–PD technique shows fewer damaged zone in the spillway region. Furthermore, there are no cracks or damaged zones in the upstream face of the base and abutment regions for this case, even though significant damage and cracking is observed in that region for the PD model. Therefore, it could be concluded that in general, PD approach results in unrealistic crack patterns and overestimates the degree of damage occurring in the dam body. Multiaxial stress states governed in such 3-D mass concrete structures lead to shear damages represented herein with tensile and compressive damages occurring simultaneously. Shear damage causing the softening and strength loss in compression for the damaged regions under multiaxial loadings affect the seismic safety of an arch dam and need to be carefully captured.
Overall, the DC–PD technique is proved to be a more rigorous, consistent and realistic approach from different aspects in comparison with both DC and PD models alone. This combined approach is certainly a step toward reducing the deficiencies of other simpler approaches usually employed in applications regarding nonlinear seismic analysis of concrete arch dams. In order to evaluate the real

seismic safety of concrete arch dams, the dam–foundation interaction as another important factor needs to be also included. The dam response is commonly overestimated due to ignoring the radiation effects in the foundation. Neglecting such a factor in the seismic safety analysis retains a sufficient safety margin in the design, because it usually reduces the response mainly due to adding a radiation damping to the system. It needs further investigation in the future.

ACKNOWLEDGMENTS

The supports of the elite National Foundation and the Ministry of Science, Research and Technology of Iran are greatly appreciated. The writers also thank Professor Somasundaram Valliappan for insightful discussions during the first author's visit to the University of New South Wales, Sydney, Australia.

REFERENCES

Ahmadi, M.T. and Razavi, S. (1992). A three-dimensional joint opening analysis of arch dam. *Computers and Structures*. **44:1/2**, 187-192.

Ahmadi, M.T., Izadinia, M. and Bachmann, H. (2003). A discrete crack joint model for nonlinear dynamic analysis of concrete arch dams. *Computers and Structures*. **79**, 403-420.

Arabshahi, H.R. and Lotfi, V. (2009). Nonlinear dynamic analysis of arch dams with joint sliding mechanism. *Engineering Computations*. **26**:5, 464-482.

Azmi, M. and Paultre, P. (2002). Three-dimensional analysis of concrete dams including contraction joint non-linearity. *Engineering Structures*. **24**, 757-771.

Chopra, A.K. (2008). Earthquake analysis of arch dams: factors to be considered. 14th World Conference on Earthquake Engineering, Beijing, China.

Espandar, R., Lotfi, V. and Razaqpur, G. (2003). Influence of effective parameters of non-orthogonal smeared crack approach in seismic response of concrete arch dams. *Canadian Journal of Civil Engineering*. **30**, 890-901.

Fenves, G.L., Mojtahedi, S. and Reimer, R.B. (1992). Effects of contraction joints on earthquake response of an arch dam. *Journal of Structural Engineering, ASCE*. **118:4**, 1039-1055.

Gunn, R.M. (2001a). Nonlinear design and safety analysis of arch dams using damage mechanics, part 1: formulation. *Hydropowers and Dams*. **2**, 67-74.

Gunn, R.M. (2001b). Nonlinear design and safety analysis of arch dams using damage mechanics, part 2: applications. *Hydropowers and Dams*. **3**, 72-80.

Lau, D.T., Noruziaan, B. and Razaqpur, A.G. (1998). Modeling of contraction joint and shear effects on earthquake response of arch dams. *Earthquake Engineering and Structural Dynamics.* **27**, 1013-1029.

Lee, J. and Fenves, G.L. (1998a). A plastic–damage model for cyclic loading of concrete structures. *Journal of Engineering Mechanics, ASCE*. **124**, 892-900.

Lee, J. and Fenves, G.L. (1998b). A plastic–damage model for earthquake analysis of dams. *Earthquake Engineering and Structural Dynamics*. **27**, 937-956.

Lee, J. and Fenves, G.L. (2001). A return-mapping algorithm for plastic–damage models: 3-D and plane stress formulation. *International Journal for Numerical Methods in Engineering*. **50**, 487–506.

Lotfi, V. and Espandar, R. (2004). Seismic analysis of concrete arch dams by combined discrete crack and non-orthogonal smeared crack technique. *Engineering Structures*. **26**, 27-37.

Lubliner, J., Oliver, J., Oller, S. and Onate, E. (1989). A plastic–damage model for concrete. *International Journal of Solids and Structures.* **25**, 299-326.

Mirzabozorg, H. and Ghaemian, M. (2005). Nonlinear behavior of mass concrete in three-dimensional problems using a smeared crack approach. *Earthquake Engineering and Structural Dynamics*. **34**, 247-269.

Omidi, O. (2010) .SNACS: A program for Seismic Nonlinear Analysis of Concrete Structures. Department of Civil and Environmental Engineering, Amirkabir University of Technology, Tehran, Iran.

Omidi, O. and Lotfi, V. (2007). Application of pseudo–symmetric technique for seismic analysis of concrete arch dams. *Fourth International Conference on Fluid–Structure Interaction.* **Vol I:** 153-162.

Omidi, O. and Lotfi, V. (2010). Finite element analysis of concrete structures using plastic–damage model in 3-D implementation. *International Journal of Civil Engineering.* **8:3**, 187-203.

Omidi O. and Lotfi V. (2012) .Continuum large cracking in a rate-dependent plastic–damage model for cyclic-loaded concrete structures. *International Journal for Numerical and Analytical Methods in Geomechanics*. Accepted for publication.

Valliappan, S., Yazdchi, M. and Khalili, N. (1999). Seismic analysis of arch dams – a continuum damage mechanics approach. *International Journal for Numerical Methods in Engineering*. **45**, 1695-1724.